Electron spatial localization tuned by strain in Ge/Si quantum dot heterostructures

A. F. Zinovieva,[1,2,*] V. A. Zinovyev,[1] A. V. Nenashev,[1,2] L. V. Kulik,[2,3] and A. V. Dvurechenskii[1,2]
[1]*Rzhanov Institute of Semiconductor Physics, SB RAS, 630090 Novosibirsk, Russia*
[2]*Novosibirsk State University, 630090 Novosibirsk, Russia*
[3]*Institute of Chemical Kinetics and Combustion, SB RAS, 630090 Novosibirsk, Russia*

(Received 25 July 2018; revised manuscript received 8 February 2019; published 22 March 2019)

A new type of quantum dot (QD) structure that enables us to control a spatial localization of electrons by changing the strain distribution in the vicinity of QDs is proposed. The structures represent a combination of large (∼200 nm) GeSi disklike quantum dots (nanodisks) and groups of smaller (∼30 nm) laterally ordered QDs grown over a nanodisk template. Electron localization has been studied by the electron spin resonance (ESR) method. Analysis of experimental results has been supported by calculations of electron binding energies and carrier distribution probabilities taking into account strain effects and real geometry of nano-objects. Results show that the strain field produced by the nanodisk can be used for tuning the energy levels of electrons in different Δ valleys and makes possible successful realization of simultaneous localization of two electrons with different g factors in the vicinity of the same QD.

DOI: 10.1103/PhysRevB.99.115314

I. INTRODUCTION

New trends in electronics demand the development of semiconductor nanostructures with controllable optical and spin properties. One of the most promising systems for manipulating an electronic structure of nano-objects is a Ge/Si heterosystem with self-assembled quantum dots (QDs) grown by molecular beam epitaxy (MBE). In this system the strain induced by lattice mismatch has a strong effect on the energy spectrum of charge carriers localized at QDs. The Ge/Si(100) QDs exhibit a type-II band lineup. The large (∼0.7 eV) valence band offset leads to an effective localization of holes in Ge regions, which represent potential barriers for electrons. However, the strain makes possible the electron localization in the Si vicinity of Ge QDs. In the case of small QDs with lateral size $L \sim 10$–20 nm, which are usually pyramidal, electrons are localized at the apexes of QDs [1,2], where the largest strain is realized [3]. For larger QDs ($L \geqslant 30$ nm) electrons can be localized also at QD base edges [4,5]. The strain difference in these localization areas can provide a change of such spin properties as a g factor [4,6] and a spin relaxation time and leads to an improvement of optical characteristics, for example, a light emitting probability. For example, the localization of electrons at QD base edges leads to a sevenfold increase of photoluminescence intensity from Ge/Si QD structures [7].

The most attractive application of QD systems with controllable electron localization is a quantum computation. Until recently, a scheme with one confined electron per QD has been considered as a basic scheme in quantum computing with QDs [8]. However, new results obtained by the electron spin resonance (ESR) method for disklike GeSi QDs (nanodisks) with lateral size $L \sim 200$–250 nm demonstrate that this type of QD can hold two electrons with different g factors [6]. Electrons can be localized in different spatial regions near GeSi nanodisks (NDs): at the top edges and at the base edges of NDs, and the g-factor difference derives from the electron localization in different Δ valleys. The localization at the top edges of the NDs has the same nature as the localization of electrons at the apexes of pyramidal QDs [2]. Principally, these two electrons can be considered as a pair of qubits with a constant exchange coupling, but there are some obstacles in the way. The lateral size of disklike GeSi QDs is too large [9], and the exchange coupling of electrons is negligible (the distance between electron states is about 50 nm). Recently, a method for implementation of quantum logic gates has been proposed for two coupled electrons with different g factors [10]. The numerical experiments give the optimal parameters: g-values difference $\delta g = 5 \times 10^{-4}$ and exchange interaction $J = 10^{-10}$ eV, providing the minimal error of quantum logic operations. The optimal QD shape that meets these requirements is a *hut* cluster with a short base size being close to 30 nm. Such kinds of QDs were investigated recently by the ESR method, but a simultaneous localization of two electrons was not achieved [11]. Only one ESR signal corresponding to electrons localized at QD base edges was detected in the dark conditions. Localization of two electrons near the same QD was realized only under illumination, when the first electron was localized at the QD base edge and the second electron was localized at the QD apex due to Coulomb attraction to a photohole captured in a Ge QD. One possible reason for this failure is a strong difference in the binding energies of electrons localized at QD base edges and QD apexes. The precise tuning of the strain in the QD structure is required to reach a simultaneous localization of two electrons with different g factors near the same QD.

In the present work the combined heterostructures representing a combination of large (∼200 nm) GeSi disklike QDs and groups of smaller (∼30 nm) laterally ordered QDs

*aigul@isp.nsc.ru

grown over the nanodisks were proposed for the strain tuning and control of the electron localization in the vicinity of Ge QDs. Developed QD structures allow us to obtain a desired spatial localization of electrons and to achieve a simultaneous localization of two electrons with different g factors near the same QD. Another advantage of these combined structures is a possibility to control the nucleation sites of smaller QDs with a strain field of large nanodisks. One can obtain the different configurations of QDs and grow the QD groups with different sizes and coupling between QDs by changing the distance between NDs and smaller QDs.

II. DESIGN OF Ge/Si QD STRUCTURES

Strain is the main factor providing an electron localization in Ge/Si QD structures. In the absence of strain electrons can be localized in the Ge/Si QD system only under illumination due to Coulomb attraction to photoholes localized in Ge QDs. The strain produced by Ge QDs forms the potential wells for electrons in Si environment. In the case of Ge QDs grown on the Si(001) substrate, the strain induces the splitting of the sixfold degenerated conduction band edge in Si at Δ point [12]. Since the strain distribution is inhomogeneous, this splitting varies from place to place in the Si surrounding. Near the QD apex the strain in Si is close to an uniaxial compression along the growth direction [001] that results in the formation of the potential wells for electrons in Δ^{001} and $\Delta^{00\bar{1}}$ valleys (Δ_z valleys). Near the QD base edge the strain in Si is close to an uniaxial compression along the in-plane direction perpendicular to this QD base edge. Such strain results in the formation of potential wells for electrons in the in-plane Δ valleys, for example, in Δ^{010} and $\Delta^{0\bar{1}0}$ valleys (Δ_y valleys) for the QD base edge along [100] direction (see the scheme of electron localization in Ref. [4]). However, electrons can be localized at the QD base edge only if the length of this edge exceeds some critical value $L \geqslant 30$ nm. For a shorter base edge the potential well will be too narrow and the binding energy E_b of an electron in Δ_y valley will be smaller than E_b of an electron in Δ_z valley. Then for small QDs the localization of electrons at QD apexes is typical. In contrast, for QDs with a lateral size exceeding 30 nm the localization at the QD base edges is more prevalent. Especially, such type of electron localization is realized in most cases, if the large QDs are covered by Si at temperatures higher than 400 °C. This is due to intensive Ge-Si intermixing and smearing of the QD apex [13,14]. At overgrowth temperature $T \geqslant 500$ °C the apex electron localization can be realized only under illumination due to Coulomb attraction to photoholes captured in Ge QDs. Then it is better to keep the temperature of the QD overgrowth no higher than 450 °C, but no lower than 400 °C, to avoid the generation of point defects in the growing layer [15,16].

Based on the existing experimental results [4,6] we select the growth conditions enabling us to obtain QD structures with desired parameters. Compact groups of QDs having a *hut*-cluster shape can be grown on the strain-modulated substrate with large GeSi nanodisks embedded under the Si surface [9,17]. Strain field produced by the large GeSi disk in the Si surface layer governs the diffusion of adatoms and provides the nucleation of Ge islands just over most tensile strained surface regions [18]. It is possible to control the size

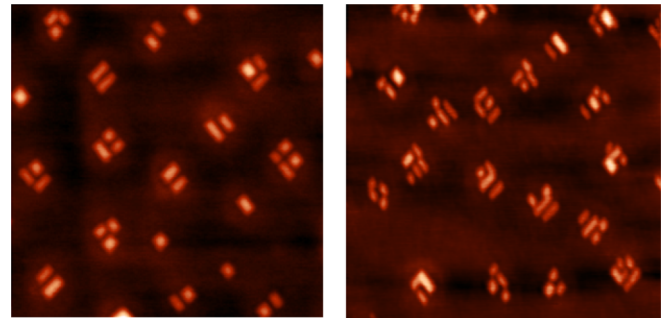

FIG. 1. AFM image (1×1 μm^2) of the compact QD groups grown by deposition of 5 monolayers (ML) of Ge at 600 °C (left panel) and 5.5 Ge ML at 580 °C (right panel) on the substrate with GeSi nanodisks, incorporated under the surface at the depth of 35 nm and serving as templates for nucleation of these ordered QD groups. Image sides are oriented along ⟨110⟩ directions.

and number of QDs in the group by changing the distance between the GeSi disk and the nucleating QD group [19,20]. For example, QD groups grown at 600 °C just on the surface of the embedded GeSi disk consist of four *hut* clusters with short base size $L_x \approx 50$ nm [9], while QD groups grown at the distance of 35 nm from the nanodisk contain mainly two or three *hut* clusters having $L_x \approx 35$ nm (Fig. 1, left panel). A slight decrease in the growth temperature (down to 580 °C) allows us to form *hut* clusters with $L_x \approx 30$ nm (Fig. 1, right panel). The last parameter satisfies fully our demands and therefore we have studied QD groups grown at the distance of 35 nm from the template disk layer at 580 °C (Fig. 2). As one can see in Fig. 1, the change of the growth temperature does not lead to a principal modification of the QD group geometry, providing only an increase of QD number in groups. The groups with three or more QDs become predominant on the surface of the growing layer (see Fig. 1, right panel). The deposition of 5.5 ML of Ge at 580 °C results in the formation of QD groups with density 2×10^9 cm^{-2}, while the surface density of the QDs is about $\simeq 10^{10}$ cm^{-2}.

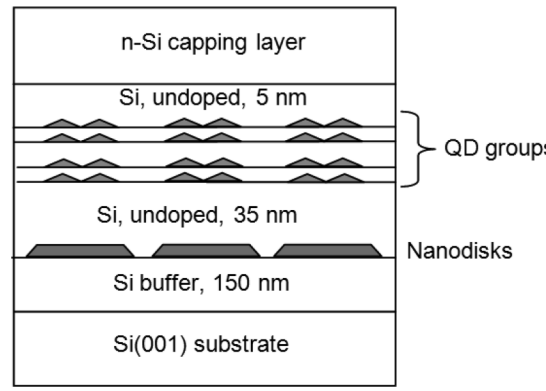

FIG. 2. A schematic structure of the sample with optimal configuration of QDs for observation of simultaneous localization of electrons in different Δ valleys. The first and second QD layers as well as the third and fourth QD layers are separated by 3 nm Si spacers, while the distance between the second and third QD layers is 5 nm.

TABLE I. Binding energies E_b of electrons in different Δ valleys localized in QD structures with a different number of vertically aligned QD pairs. Here ND is an abbreviation for nanodisk. d is the thickness of the Si layer between QD layers in the stack. Notation "Double QD pairs" corresponds to a two-layered QD structure. Notations "QD pairs/ND," "QD stack/ND" are used for the description of structures with QD layers grown on an ND template. All QD stacks are four layered. The site numeration corresponds to Fig. 3.

	E_b (meV)				
Type	Δ_z (site 1)	Δ_z (site 2)	$\Delta_{x,y}$ (site 3)	Δ_z (site 4)	$\Delta_{x,y}$ (site 5)
Double QD pairs $d = 3$ nm	27	–	40	–	–
Double QD pairs/ND $d = 3$ nm	36	–	35	18	24
QD stack $d = 3$ nm	49	–	82	–	–
QD stack/ND $d = 3$ nm (sample 907)	56	–	76	18	24
QD stack $d = 3, 5, 3$ nm	44	43	66	–	–
QD stack/ND $d = 3, 5, 3$ nm (sample 937)	51	52	61	18	24

To increase the binding energy of electrons, the growth of stacked QD structure with a strain accumulation from different QD layers should be used. The more QD layers there are in the stack, the bigger the electron binding energy is. To define the optimal number of QD layers in the stack, we calculate the energy spectrum of electrons in the model structures with different number of QD layers and ND layers (see Table I). We use the program Nextnano^3 [21], allowing us to take into account the strain effects and the real geometry of nanoobjects. All electron energies are obtained in a one-electron approximation. The calculation of the strain distribution is performed using analytical expressions developed in the work [22] and program Easystrain3d [23] that reduces significantly (by orders of magnitude) the calculation time. Since the size of the calculation cell is large ($300 \times 300 \times 120$ nm^3), the efficiency gain actually is very huge. Such improvement is possible due to the flexibility of the program Nextnano^3 working with external strain data, as well as with its own solver of the elasticity problem.

The geometry and Ge content of QDs are taken according to experimental data obtained by scanning tunneling microscopy (STM), atomic force microscopy (AFM), transmission electron microscopy [17], and extended x-ray absorption fine structure (EXAFS) spectroscopy [24]. The shape of nanodisks is described by the truncated cone with bottom diameter $D_b = 250$ nm, top diameter $D_t = 200$ nm, and height $h_{\mathrm{ND}} = 10$ nm. Ge content in nanodisks is taken to be equal to 35%. The smaller QDs have the shape of *hut* clusters oriented along ⟨100⟩ directions. Their height is $h_{\mathrm{QD}} = 2.5$ nm, the size of the short base edge is $L_x = 35$ nm, and the size of the long base edge is $L_y = 70$ nm. The inclination angle of side facets α is taken so that $\tan\alpha = 0.2$, which corresponds to facet orientation {105}. The Si spacer thickness between layers of QD groups is varied from 3 to 5 nm depending on the type of calculated structure. Ge content in *hut* clusters is taken to be equal 50%. The main part of the calculations is performed for the structures with QD groups representing in-plane pairs of coupled QDs. A gap between aligned base edges of QDs in pairs (in x direction, Fig. 5) is taken to be equal to 3 nm. To verify how an increase of QD number in the group affects the modeling results we calculate also the energy spectrum of electrons in the structures with groups of three QDs with a smaller QD width $L_x = 30$ nm and the same separating distance. In general, the energy level disposition has not changed. The increase in QD number has led only to a slight shift of the energy levels (by ≈2 meV), providing an increase in the binding energies of electrons in all Δ valleys.

The number of QD layers in the stack defines the initial depth of potential wells and the energy levels of QD electrons, which then can be tuned by the strain field of the ND. The binding energy of QD electrons should be larger than the binding energy of an electron at the donor impurity (in our experimental structures the donor impurity is Sb, with binding energy of electrons $E_b \approx 43$ meV) [25]. Electrons should leave Sb atoms and be localized in QD layers. These transitions can be prevented by the band bending induced by the space charge of Sb ions. However, a simple estimation shows that this effect is negligible (≃1 meV) at given density of QDs (≃10^{10} cm^{-2}, see Fig. 1) and distance between QDs and ionized donors (≃10 nm). This estimation was made assuming that each QD holds one electron.

Results of calculations show that a double layered QD structure does not provide a sufficient strain for electron localization in QD layers (see Table I). The binding energy of electrons in the deepest potential well does not exceed 40 meV [the energy is counted from the conduction band (CB) edge in nonstrained Si].

It is interesting that the strain in Si above the top of the GeSi nanodisk is not favorable for electron localization at the edges of QDs (in $\Delta_{x,y}$ valleys). For example, in the double layered QD structure without ND the binding energy E_b of an electron at the QD base edge (analog of site 3 shown in Fig. 3) is 40 meV, while for the same QD structure with ND layer, $E_b = 35$ meV. In the same conditions the binding energy of an electron at the QD apex (analog of site 1 shown in Fig. 3) increases from 27 to 36 meV (see Table I). Since a ND addition results in the opposite shifts of energy levels of electrons in different Δ valleys, then NDs can be used to tune the energy levels of electrons in QD layers. So, the large nanodisks can be used not only for arrangement of small QDs in compact groups, but to achieve the optimal energy level disposition for the simultaneous localization of electrons in different Δ valleys.

Strain in the structures with four layers of QD groups provides an effective localization of electrons in QD layers. The calculation results demonstrate that a four-layered QD stack with spacer thickness $d = 3$ nm provides a binding energy $E_b = 76$ meV (see Table I) for an electron at the QD base edge (site 3 in Figs. 3 and 4). The maximum of electron finding probability is found in the center of

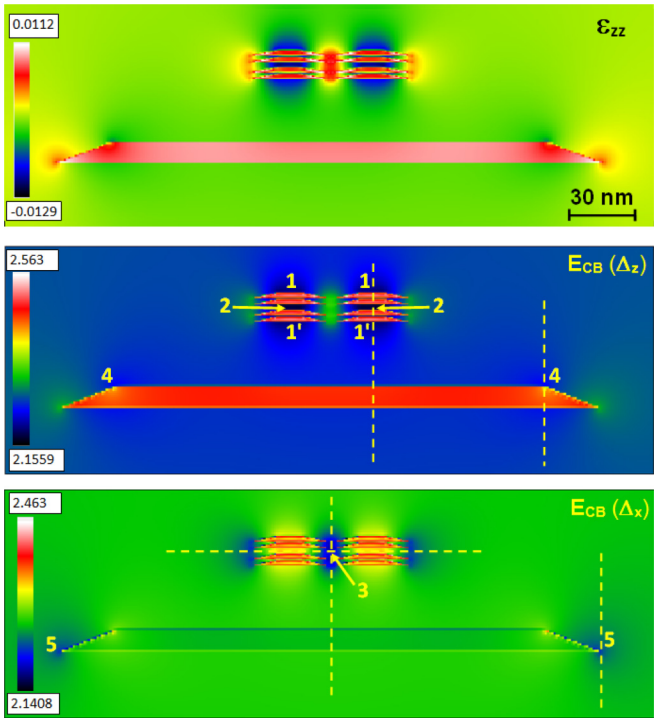

FIG. 3. Strain distribution (top panel), conduction band edge landscape in Δ_z valley (center panel), and conduction band edge landscape in Δ_x valley (bottom panel) in the structure with optimal configuration of QDs for observation of simultaneous localization of electrons in different Δ valleys. Sections of XZ plane passing through the center of the compact QD group are shown, Z is the growth direction of the structures [001].

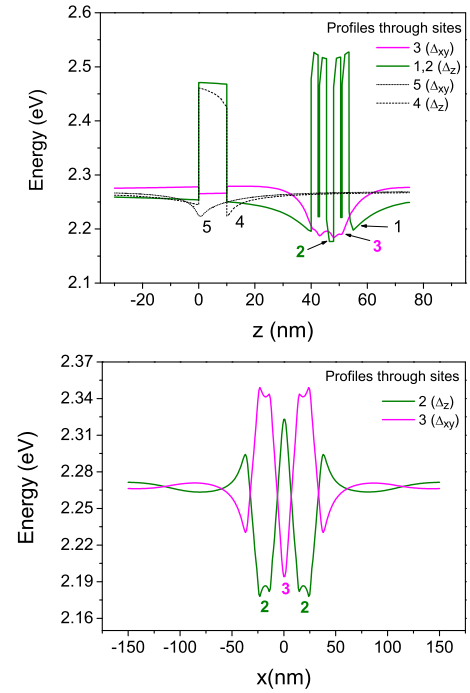

FIG. 4. Z profiles (top panel) and X profiles (bottom panel) of conduction band edge, crossing through sites 1, 2, 3, 4, 5 (profile directions are shown by dashed lines in Fig. 3). Profiles through sites 1, 2, 4 are related to Δ_z valley, profiles through sites 3 and 5 correspond to Δ_x valley.

the stacked structure, between the longest *hut*-cluster edges (Fig. 5). The electron in Δ_z valley is localized near the apex of the *hut* cluster in the top QD layer (site 1) with $E_b = 56$ meV. However, such disposition of electron states cannot provide a sufficient exchange coupling between electrons in Δ_z valley and $\Delta_{x,y}$ valleys. The best condition for exchange coupling is the localization of the apex electron in the center of the QD stack. For this purpose we consider a four-layered QD stack with central spacer thickness increased up to 5 nm, grown on the template structure with one ND layer. For this structure the calculations give the optimal spatial arrangement of electrons from different Δ valleys (Fig. 5). An electron in Δ_x valley is localized at QD edges in the vertical Si gap (site 3) with $E_b = 61$ meV, while an electron in Δ_z valley is localized in the central Si spacer (site 2) with $E_b = 52$ meV (see the last row in Table I).

So, the last QD configuration is optimal for the simultaneous localization of two electrons from different Δ valleys. Both electrons can be localized simultaneously despite the Coulomb repulsion between them. To demonstrate this we calculate the energy of the next electron in the presence of the first electron localized at QD base edges (site 3). To model this situation we add to the Hamiltonian the term $U_c = e^2/[4\pi\varepsilon\varepsilon_0\sqrt{(x-x_0)^2+(y-y_0)^2+(z-z_0)^2+a^2}]$, where $\varepsilon = 12$ is the relative permittivity of Si, (x_0, y_0, z_0) is the position of the first electron wave function maximum (at site 3), a is the smallest radius of this wave function (along x direction), and $a = a_x = 2$ nm. The results of the calculations show that in these conditions the additional electron can be localized at site 3 with $E_b = 48$ meV, and the next electron is localized at site 2 with $E_b = 47$ meV. So the energy of the Coulomb repulsion U_{33} between the electrons at site 3 is close to 13 meV, while the energy of the Coulomb repulsion U_{23} between an electron at site 2 and an electron at site 3 is close to 5 meV (the distance between sites 2 and 3 is $l_{23} \approx L_x/2 \approx 17$ nm). It should be noted that this calculation overestimates the value of U_{33}, because the wave function of the electron at site 3 has the larger characteristic sizes along y and z directions ($a_y \approx 7.5$ nm, $a_z \approx 3.5$ nm, see Fig. 5). Also, the presence of Ge layers between electrons should be taken into account. Since the relative permittivity of Ge is larger [$\varepsilon(Ge) = 16$], then the Coulomb interaction between electrons will be smaller. So, the energy level shift due to Coulomb interaction will be slightly smaller and all three electrons (two electrons at site 3 and one electron at site 2) can be localized together in the dark conditions (their binding energies are larger than the E_b of the electrons localized on Sb donors).

For electrons localized at the top of the QD stack (site 1), the initial (without Coulomb interaction) binding energy is 51 meV, while in the presence of the first electron at site 3 this energy reduces down to 46 meV. Moreover, there is a Coulomb interaction with an electron localized at site 2, leading to a decrease in the binding energy. The distance between site 1 and site 2 is only 6 nm (much smaller than l_{23}), so we expect a stronger effect than for sites 2 and 3 (> 5 meV). Therefore, in experiments this state can be

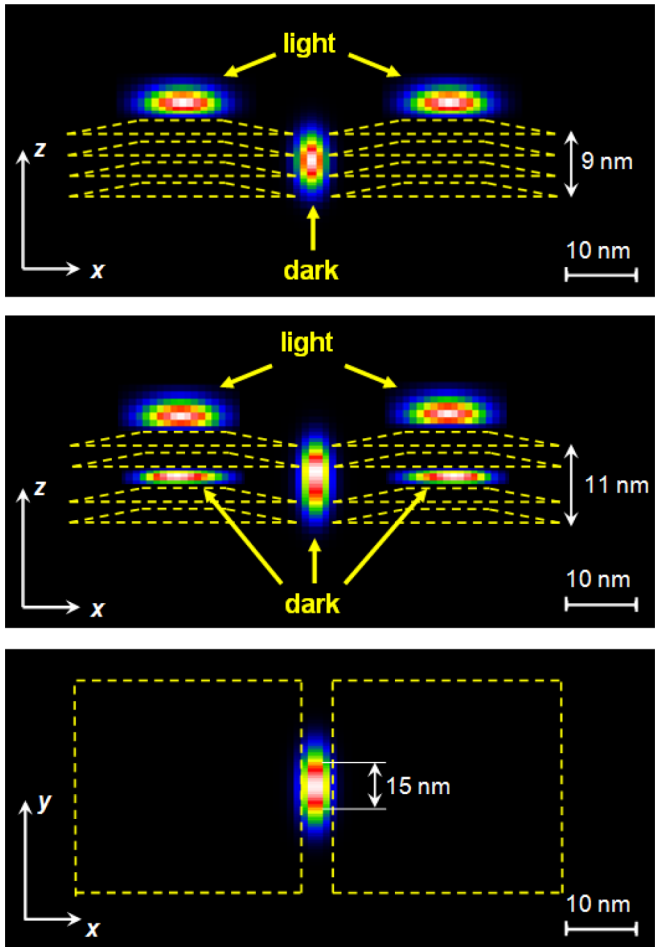

FIG. 5. Wave functions of the electron ground state in Δ_x valley (located at the QD edges) and electron ground state in Δ_z valleys (located at the QD apexes) in different QD structures: with constant spacer thickness $d = 3$ nm (top panel) and with varied spacer thickness $d = 3, 5, 3$ nm (center panel). Sections of XZ plane passing through the center of the compact QD group are shown (top and center panels). Section of XY plane passing through the base of third QD layer ($z_0 = 48$ nm). The conditions of experimental observation are indicated (dark or light). QD geometry is shown by dashed lines. The scales in x, y, z directions are different.

detected only under illumination (see experimental results below). It should be noted that there is an analogous potential well in Δ_z valley (site $1'$, see Fig. 3), where electrons can also be localized under illumination. According to our calculations the binding energy of an electron at this site is slightly smaller (by $\approx$0.7 meV) than the E_b of an electron at site 1.

Electrons at sites 4 and 5 also cannot be detected in experiments, because they have very small binding energy, 18 and 24 meV, correspondingly (for the structures with one-layer ND template).

III. SAMPLES AND EXPERIMENT

Guided by preliminary calculation results we grew the experimental structures by MBE on n-Si(001) substrates with a resistivity $\geqslant 1000\ \Omega$ cm. First, a 100 nm buffer Si layer was grown at $T = 500\,^{\circ}$C. The nanodisk layer was grown by deposition of 7.5 ML of Ge at 700 °C. Then a 35 nm Si spacer layer was grown at 700 °C. Each QD group layer was grown at the temperature $T_{QD} = 580\,^{\circ}$C. The first QD layer was formed by deposition of 5.5 Ge ML. The Ge QDs formation in each subsequent layer was controlled by reflection high energy electron diffraction (RHEED). A moment, when the pattern changes from streaky to spotty, is considered as the beginning of three-dimensional island formation, after which 0.3 ML of Ge was deposited additionally. Such a procedure provides an almost equal size of Ge QDs in all layers of the stacked structure [26,27].

Two structures with four-layered QD stacks differing in thickness of spacer layers were grown: (1) with 3 nm Si spacer layers between all QD layers (structure 907), and (2) with 5 nm central spacer layer and 3 nm spacer layers between the first and second QD layers and the third and fourth QD layers as depicted in Fig. 2 (structure 937). Si spacer layers were grown at 400 °C. The top QD layer was covered by 5 nm Si layer also at 400 °C. Finally, all structures were covered at 500 °C by a 195 nm Si layer doped by Sb with concentration $\simeq 5 \times 10^{16}$ cm^{-3} to supply QD layers by electrons.

Also a test structure without QDs and NDs was grown in identical growth conditions. The structure represents a 200 nm Si layer with the same Sb concentration grown on a 100 nm Si buffer layer at 500 °C.

We studied the ESR using a standard Bruker X-band spectrometer operating at a frequency close to 9.7 GHz at sample temperatures ranging from 4.5 to 30 K. The samples represent rectangular plates with size 4×12 mm^2 cut along the principal crystalline directions [110] and [$\bar{1}$10]. Two samples are glued on a quartz holder, allowing a rotation in the magnetic field, and then the entire cavity and samples were maintained at low temperature with a helium flow cryostat (Oxford CF935). The interfering ESR signal from the Si dangling bonds ($g = 2.0055$) was eliminated using passivation of structures with atomic hydrogen before measurements. The absolute accuracy of the g value determination was ± 0.0001. The relative accuracy of measurements was increased by about one order of magnitude using g-factor standards. All g-factor values were calibrated to the conduction electron g factor of the Li metal particles in LiF [28]. Also we use a heavily P-doped silicon sample with a phosphorus concentration $\sim 5 \times 10^{18}$ cm^{-3} as an additional g-factor standard [29]. Some experiments are performed with a continuous illumination produced by the tungsten-halogen lamp through the optical access windows in the cryostat and resonator.

IV. RESULTS AND DISCUSSION

The experimental results demonstrate that the spatial localization of electrons can be controlled by parameters of combined QD structure. ESR spectra obtained on the structures with different spacer thickness in the QD stack reveal that electrons in these structures are localized in different spatial regions near Ge/Si QDs.

Sample 937 with varied spacer thickness demonstrates in the dark two ESR signals (Fig. 6) with g factors $g_{zz}^{(1)} = 1.9987$ and $g_{zz}^{(2)} = 1.9993$ (in the magnetic field applied along the growth direction [001]). The ESR linewidths are $\Delta H_{pp}^{(1)} \approx 0.8$ Oe and $\Delta H_{pp}^{(2)} \approx 0.6$ Oe, respectively, and do

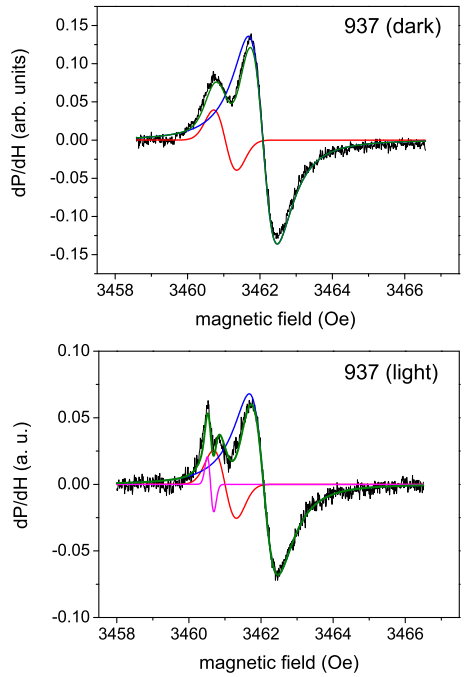

FIG. 6. ESR signals observed in the dark (top panel) and under continuous illumination (bottom panel) for the heterostructure with four layers of ordered QD groups, separated by 3 nm bottom and top Si spacer layers and 5 nm central Si spacer, grown on the template with one GeSi nanodisk (No. 937). Microwave power $P =$ 0.063 mW and frequency $\nu = 9.68484$ GHz, modulation amplitude $H_m = 0.3$ Oe, $T = 5$ K. The magnetic field is directed along the growth direction of the nanostructure.

not change with the sample rotation in the magnetic field. The angular dependencies of g factors are typical for electrons in different Δ valleys [4] (Fig. 7). In the tilted magnetic fields the ESR signal with $g_{zz} = 1.9993$ shifts to the range of higher magnetic fields, showing the behavior typical for ESR signals from electrons in Δ_z valley. The signal with $g_{zz} =$ 1.9987 shifts towards the first one, which indicates its origin

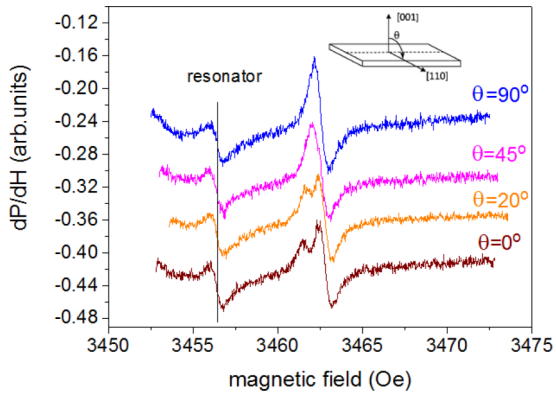

FIG. 7. ESR spectra of electrons localized in the structure with modulated spacer thickness (No. 937) for different sample orientations in the magnetic field, microwave power $P = 0.063$ mW and frequency $\nu = 9.68694$ GHz, modulation amplitude $H_m = 0.3$ Oe, $T = 5$ K. The magnetic field direction is changed from the growth direction of the structure ($\theta = 0^\circ$) to the in-plane direction [110].

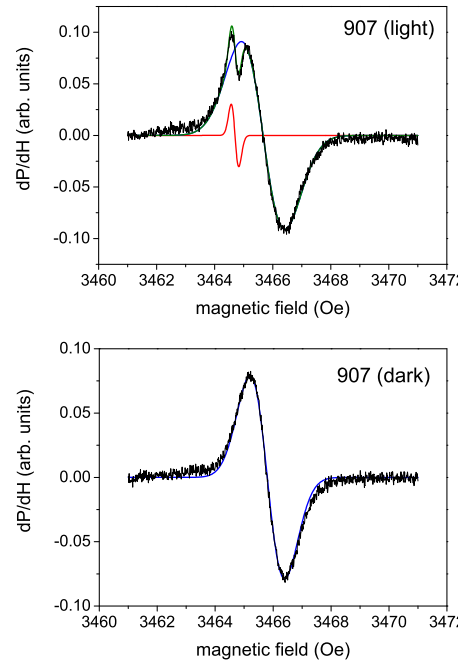

FIG. 8. ESR signals observed in the dark and under continuous illumination for the heterostructure with four layers of ordered QD groups, separated by 3 nm Si spacer layers, grown on the template with one GeSi nanodisk (No. 907). Microwave power $P =$ 0.063 mW and frequency $\nu = 9.69673$ GHz, modulation amplitude $H_m = 0.3$ Oe, $T = 5$ K. The magnetic field is directed along the growth direction of the structure.

from electrons in $\Delta_{x,y}$ valleys. After $\theta = 45^\circ$ ESR signals became indistinguishable and one signal with $g = 1.9989$ was observed at $\theta = 90^\circ$.

Under illumination of sample 937 the third ESR signal with g-factor $g_{zz}^{(3)} = 1.9995$ and $\Delta H_{pp}^{(3)} \approx 0.2$ Oe appears. In the magnetic field applied along the growth direction all three ESR signals are well distinguishable (see line approximation in Fig. 6, bottom panel). With deviation of the magnetic field from this direction the additional light-induced ESR signal also shifts, like a signal from the electrons in Δ_z valley, to the range of higher magnetic fields. For the in-plane magnetic field all signals overlap and represent one ESR signal as in the dark.

Sample 907 with equal Si spacer layers in the QD stack demonstrates in the dark one ESR signal with $g_{zz} = 1.9990$ and an isotropic ESR linewidth $\Delta H_{pp} \approx 1.2$ Oe. Under illumination the second ESR signal with $g_{zz} = 1.9995$ and $\Delta H_{pp} \approx 0.25$ Oe appears (Fig. 8). In the tilted magnetic fields the light-induced signal shifts to the range of higher magnetic fields while the position of the first signal remains unchanged. At $\theta = 45^\circ$ signals overlap like for sample 937.

The test structure without QDs and NDs demonstrates an isotropic ESR signal with $g_{zz} = g_{\text{in-plane}} = 1.99856$ ($g_{\text{in-plane}}$ corresponds to the in-plane magnetic field applied along [110] direction). The signal has ESR linewidth $\Delta H_{pp} = 1.3$ Oe typical for Sb donors [29]. We have studied the microwave power dependence of this ESR signal and compared it with the power dependence of the ESR signal with the closest g value, $g_{zz} = 1.9987$, observed for QD structures. The ESR signal

TABLE II. g_{zz} values of electrons in Δ_z valley and $\Delta_{x,y}$ valleys in the structures under study. Here $\delta g = g_{zz}(\Delta_z) - g_{zz}(\Delta_{x,y})$.

No.	g_{zz} (Δ_z, site 1)	g_{zz} (Δ_z, site 2)	g_{zz} ($\Delta_{x,y}$, site 3)	max(δg)
907 light	1.9995	–	1.9990	0.5×10^{-3}
907 dark	–	–	1.9990	
937 light	1.9995	1.9993	1.9987	0.8×10^{-3}
937 dark	–	1.9993	1.9987	0.5×10^{-3}

from QD structures saturates at microwave power $P = 0.63$ mW (25 dB), while the signal from the test structures saturates at $P = 6.3$ mW (15 dB).

The experimental results can be explained based on the calculation of the energy spectra and an analysis of angular dependencies of g factors. As it was mentioned in the classical work of D. K. Wilson and G. Feher [30], if all electrons in the sample are located in one separated Δ valley, one should detect the ESR signal with a special angular dependence of g factor reflecting the symmetry of this valley (an ellipsoid of revolution). Then for electrons in Δ_z valley the g factor in the magnetic field applied along [001] direction should coincide with $g_\parallel = 1.9995$. And for electrons in $\Delta_{x,y}$ valleys the g factor in the same conditions should coincide with $g_\perp = 1.9984$, where $g_\parallel$ and $g_\perp$ are longitudinal and transverse components of an electron g tensor for a chosen Δ valley [25]. With deviation of a magnetic field from [001] direction a g-factor behavior for electrons in Δ_z valley is described as $g = [g_\parallel^2 \cos^2(\theta) + g_\perp^2 \sin^2(\theta)]^{1/2}$, where θ is the angle between the magnetic field direction and Z axis. For the in-plane magnetic field electrons in $\Delta_{x,y}$ valleys have g value defined by angle φ between the magnetic field and the major valley axis along [010] direction: $g = [g_\parallel^2 \cos^2(\varphi) + g_\perp^2 \sin^2(\varphi)]^{1/2}$. In experiments the in-plane magnetic field is applied along [110] direction, then $g_{\text{in-plane}} = 1.9990$ for $\Delta_{x,y}$ valleys electrons. The g-factor angular dependence observed for the structures under study is fully described within this approach and allows us to make an assignment of the signals. It should be noted that the g-factor anisotropy observed in the works [31–33] has a different nature and is related to the spin-orbit interaction induced by an asymmetry of the structures (Rashba or Dresselhaus terms). In these works [32,33] another in-plane anisotropy of g factor was observed. The absence of Rashba effects in our structures is confirmed by the isotropy of ESR linewidths. Usually, in two-dimensional asymmetrical structures, the ESR linewidth becomes anisotropic, ESR lines are broadened with the sample rotation in the magnetic field [31]. In our case all ESR linewidths are isotropic.

For sample 937 we attribute the ESR signal with $g_{zz} = 1.9993$ to electrons localized at site 2, the ESR signal with $g_{zz} = 1.9987$ to electrons localized at site 3, and the light-induced signal with $g_{zz} = 1.9995$ to electrons localized at site 1 (see Table II). The first value of g_{zz} turns out to be slightly smaller that expected value $g_{zz} = 1.9995 \pm 0.0001$. We suppose that the reason is the presence of Ge atoms in the localization area of electrons (site 2). This potential well is very narrow and an electron wave function is strongly confined between $Ge_{0.5}Si_{0.5}$ barriers. The wave function penetration into barriers provides the obtained g factor. Similar decreasing of g_{zz} value for electrons at the apexes of QDs was observed in Ref. [34]. In all sample electrons localized at site 3 have larger values of g_{zz} than expected for electrons in $\Delta_{x,y}$ valleys $g_{zz} = 1.9984 \pm 0.0001$. The difference is more pronounced for sample 907 ($g_{zz} = 1.9990$). Also, for sample 907 the anisotropy of the g value of electrons localized at site 3 completely disappears. All these effects can be related to a larger strain in sample 907 that stimulates the Ge-Si intermixing during QD overgrowth by Si and results in the presence of Ge atoms in surrounding Si. The latter should lead to the broadening of the ESR lines, which is observed for sample 907. Apparently the presence of Ge atoms provides the decreasing of g_{zz} value for electrons in Δ_z valley and the increasing of g_{zz} value for electrons in $\Delta_{x,y}$ valleys (this assumption requires theoretical verification, in particular, studies how the presence of Ge atoms affects the g factor in different Δ valleys). Overall, the difference between g factors of electrons in different Δ valleys becomes smaller in the presence of Ge atoms.

To confirm the assignment of the signals the analysis of intensities of observed ESR signals was performed. We carried out the additional experiments using the reference sample with a known number of spins and determined the number of spins for each ESR signal. This reference sample was glued to the holder and measured simultaneously with QD structures. The ESR signal from electrons at site 2 has the integral intensity corresponding to $\simeq 2 \times 10^9$ spins. Since the total area of the samples under study is approximately 1 cm^2, then this amount corresponds to 1 electron per QD group. The integral intensity of the ESR signal from electrons at site 3 corresponds to $\simeq 10^{10}$ spins (4–5 electrons per QD group). The light induced signal from the top QD electrons (site 1) has the integral intensity corresponding to $\simeq 0.2 \times 10^9$ spins. The obtained numbers of spins corresponding to electrons at sites 2 and 3 are in agreement with calculation results in order of magnitude. Nearly twofold increase of the number of electrons at site 3 as compared with simulation results can be due to a larger number of such localization centers in experimental QD groups (Fig. 1, right panel).

The potential well at site 2 can hold one electron, and according to simulations two electrons localized at these sites are expected per QD group. However, in the experiment only one of two potential wells shown in Fig. 3 was revealed in ESR spectra. We suppose that the reason is a QD size variation in real experimental structures. This potential well is very sensitive to the height of QDs, and a small deviation of this parameter from the specified one makes impossible the electron localization at this site. Some QDs in the group have slightly smaller or larger height and this can lead to decreasing the potential well depth or width and make the localization at site 2 more difficult. The situation with electron localization at site 3 is better. A slight deviation of QD parameters in the group does not lead to decreasing the number of localized electrons at site 3.

Under illumination the photogenerated holes are captured inside QDs and produce an additional attractive potential for electrons. The hole wave functions are concentrated mainly in the center of QDs, attracting the electrons to site 1. Then under illumination of sample 907 (937) the second (third) ESR

signal corresponding to electrons in the Δ_z valley appears. However, the light induced localization at site 1 was realized only in every tenth QD group. Probably, the intensity of illumination was insufficient, or charge carriers are also captured by some traps related to defects, which might be present in Si spacer layers grown at 400 °C.

Observed ESR signals cannot be related to electrons localized at nanodisks, because, as we mentioned above, the largest binding energy corresponding to electrons localized at site 4 (site 5) is only 18 meV (24 meV). The large g-factor difference, observed for the structures under study, is not peculiar to the electron localization on nanodisks. For nanodisk localization the characteristic difference in g-factors $\delta g = g(\Delta_z) - g(\Delta_{x,y}) \approx 1.5 \times 10^{-4}$ for electrons localized at sites 4 and 5 (see results of ESR study of nanodisk structures [6]).

The ESR signal from electrons at site 3 has a g_{zz} value that is very close to the g factor of electrons on Sb donors [29]. Principally, one can suppose that electrons do not leave Sb donors and remain in the Si capping layer. However, the electrons in the Sb-doped Si capping layer should have another angular dependence of the g factor. These electrons must have either an isotropic signal (as it was observed for the test sample without QDs/NDs) or demonstrate the angular dependence of the g factor typical for electrons in the Δ_z valley, because some part of the Sb atoms is found in the strain field produced by QD apexes (near the QD apex the Δ_z valley is lowest). For QD structures we do not observe these dependencies in the dark, so we think that Sb atoms are found at the larger distance from the QD layer due to their segregation typical for our growth conditions (the growth temperature for Si layer doped by Sb is 500 °C) [35]. ESR measurements performed on the test structure without QDs/NDs can be considered as an additional proof that ESR signals observed for QD structures are indeed originated from electrons localized in QD layers. Spin counting performed for the test structure show that the intensity of the ESR signal corresponds to $\approx (1.2–1.5) \times 10^{10}$ spins, which is comparable with the total intensity of ESR signals from electrons localized on QDs. So, a comparison of ESR spectra of samples with QDs and the test sample shows that practically all electrons have transferred from Sb impurities to more deep QD states.

V. CONCLUSIONS

In the present work we have developed the combined QD structures providing a simultaneous localization of two electrons with different g factors in the compact group of tunnel-coupled QDs. Structures represent a combination of large nanodisks with the lateral size ~200 nm and compact groups of *hut* clusters with the base width ~30 nm grown at the distance of 35 nm from the nanodisk layer. Strain field produced by the large nanodisk plays a pivotal role both in the spatial arrangement of compact QD groups and in the tuning of energy levels of electrons localized at QD apexes and QD base edges. The optimal parameters of QD groups provide the desired g-factor difference and optimal spatial configuration of electron wave functions. The localization of electrons was proved experimentally by the ESR method. Analysis of g values and orientational dependencies of ESR spectra allows us to perform the signal assignment. The interpretation of experimental results was supported by calculation of electron binding energies in the investigated structures with parameters of QDs obtained from AFM, transmission electron microscopy and Raman spectroscopy.

ACKNOWLEDGMENTS

This work is funded by the Russian Foundation for Basic Research (Grants No. 16-29-14031 and No. 18-52-00014), the growth of combined QD structures was carried out within the State Program of Russia (Grant No. 0306-2018-0001). The authors gratefully acknowledge V. A. Armbrister for the growth of experimental structures.

[1] A. I. Yakimov, A. V. Dvurechenskii, N. P. Stepina, A. V. Nenashev, and A. I. Nikiforov, Nanotechnology **12**, 441 (2001).

[2] A. F. Zinovieva, A. V. Dvurechenskii, N. P. Stepina, A. S. Deryabin, A. I. Nikiforov, R. M. Rubinger, N. A. Sobolev, J. P. Leitão, and M. C. Carmo, Phys. Rev. B **77**, 115319 (2008).

[3] A. V. Nenashev and A. V. Dvurechenskii, J. Exp. Theor. Phys. **91**, 497 (2000).

[4] A. F. Zinovieva, A. I. Nikiforov, V. A. Timofeev, A. V. Nenashev, A. V. Dvurechenskii, and L. V. Kulik, Phys. Rev. B **88**, 235308 (2013).

[5] D. Grützmacher, T. Fromherz, C. Dais, J. Stangl, E. Mu1ller, Y. Ekinci, H. H. Solak, H. Sigg, R. T. Lechner, E. Wintersberger, S. Birner, V. Holy, and G. Bauer, Nano Lett. **7**, 3150 (2007).

[6] A. F. Zinovieva, V. A. Zinovyev, A. V. Nenashev, L. V. Kulik, and A. V. Dvurechenskii, Z. Phys. Chem. **231**, 405 (2017).

[7] A. F. Zinovieva, V. A. Zinovyev, A. I. Nikiforov, V. A. Timofeev, A. V. Mudryi, A. V. Nenashev, and A. V. Dvurechenskii, JETP Lett. **104**, 823 (2016).

[8] D. Loss and D. P. DiVincenzo, Phys. Rev. A **57**, 120 (1998).

[9] V. A. Zinovyev, A. V. Dvurechenskii, P. A. Kuchinskaya, and V. A. Armbrister, Phys. Rev. Lett. **111**, 265501 (2013).

[10] A. V. Nenashev, A. F. Zinovieva, A. V. Dvurechenskii, A. Yu. Gornov, and T. S. Zarodnyuk, J. Appl. Phys. **117**, 113905 (2015).

[11] A. Zinovieva, N. Stepina, A. Dvurechenskii, L. Kulik, G. Mussler, J. Moers, and D. Grutzmacher, Solid State Phenom. **233–234**, 415 (2015).

[12] C. G. Van de Walle, Phys. Rev. B **39**, 1871 (1989).

[13] A. Rastelli, E. Muller, and H. von Kanel, Appl. Phys. Lett. **80**, 1438 (2002).

[14] Y. Q. Wu, F. H. Li, J. Cui, J. H. Lin, R. Wu, J. Qin, C. Y. Zhu, Y. L. Fan, X. J. Yang, and Z. M. Jiang, Appl. Phys. Lett. **87**, 223116 (2005).

[15] M. W. Dashiell, U. Denker, C. Muller, G. Costantini, C. Manzano, K. Kern, and O. G. Schmidt, Appl. Phys. Lett. **80**, 1279 (2002).

[16] U. Denker, M. Stoffel, O. G. Schmidt, and H. Sigg, Appl. Phys. Lett. **82**, 454 (2003).
[17] V. A. Zinovyev, A. F. Zinovieva, P. A. Kuchinskaya, Zh. V. Smagina, V. A. Armbrister, A. V. Dvurechenskii, O. M. Borodavchenko, V. D. Zhivulko, and A. V. Mudryi, Appl. Phys. Lett. **110**, 102101 (2017).
[18] G. Capellini, M. De Seta, C. Spinella, and F. Evangelisti, Appl. Phys. Lett. **82**, 1772 (2003).
[19] M. De Seta, G. Capellini, and F. Evangelisti, Phys. Rev. B **71**, 115308 (2005).
[20] R. Marchetti, F. Montalenti, L. Miglio, G. Capellini, M. De Seta, and F. Evangelisti, Appl. Phys. Lett. **87**, 261919 (2005).
[21] See http://www.nextnano.de/nextnano3/ for information about the program Nextnano^3.
[22] A. V. Nenashev and A. V. Dvurechenskii, J. Appl. Phys. **107**, 064322 (2010).
[23] See http://easystrain.narod.ru/ for information about strain calculation using the analytical approach.
[24] S. B. Erenburg, S. V. Trubina, V. V. Zvereva, V. A. Zinovyev, A. V. Dvurechenskii, P. A. Kuchinskaya, and K. O. Kvashnina, J. Struct. Chem. **57**, 1407 (2016).
[25] A. Dargys and J. Kundrotas, *Handbook on Physical Properties of Ge, Si, GaAs and InP* (Science and Encyclopedia, Vilnius, 1994).
[26] A. I. Yakimov, A. V. Dvurechenskii, A. I. Nikiforov, A. A. Bloshkin, A. V. Nenashev, and V. A. Volodin, Phys. Rev. B **73**, 115333 (2006).
[27] V. Le Thanh, V. Yam, P. Boucaud, F. Fortuna, C. Ulysse, D. Bouchier, L. Vervoort, and J.-M. Lourtioz, Phys. Rev. B **60**, 5851 (1999).
[28] A. Stesmans and G. van Gorp, Rev. Sci. Instrum. **60**, 2949 (1989).
[29] G. Feher, Phys. Rev. **114**, 1219 (1959).
[30] D. K. Wilson and G. Feher, Phys. Rev. **124**, 1068 (1961).
[31] Z. Wilamowski, W. Jantsch, H. Malissa, and U. Rössler, Phys. Rev. B **66**, 195315 (2002).
[32] M. Veldhorst, R. Ruskov, C. H. Yang, J. C. C. Hwang, F. E. Hudson, M. E. Flatte, C. Tahan, K. M. Itoh, A. Morello, and A. S. Dzurak, Phys. Rev. B **92**, 201401(R) (2015).
[33] R. Ferdous, E. Kawakami, P. Scarlino, M. P. Nowak, D. R. Ward, D. E. Savage, M. G. Lagally, S. N. Coppersmith, M. Friesen, M. A. Eriksson, L. M. K. Vandersypen, and R. Rahman, npj Quantum Inform. **4**, 26 (2018).
[34] A. F. Zinovieva, N. P. Stepina, A. I. Nikiforov, A. V. Nenashev, A. V. Dvurechenskii, L. V. Kulik, M. C. Carmo, and N. A. Sobolev, Phys. Rev. B. **89**, 045305 (2014).
[35] D. V. Yurasov, M. N. Drozdov, A. V. Murel, M. V. Shaleev, N. D. Zakharov, and A. V. Novikov, J. Appl. Phys. **109**, 113533 (2011).